2. 1. 4 MEBT2, ACS

2.1.4.1 ACS

We have adopted an annular coupled structure (ACS) [1] for the 190-MeV to 400-MeV part. This structure is a variation of coupled-cavity structures. The main advantage of the ACS is reduced influence of the electric field perturbation to the beam evolution [2]. In this structure, a coupling cell has a cylindrical symmetry with respect to the beam axis, and it is connected to adjacent accelerating cells with coupling slots. The existence of coupling slots generally perturbs the electric field in an accelerating cell. In the ACS, we can suppress the dipole component of the perturbation, having symmetrically placed coupling slots. Because the dipole component is expected to provide the most serious effect on beam evolution, we can reduce the slot influence to the beam evolution by adopting an ACS with adequately placed coupling slots. This is the primary reason why we chose ACS. In our case, we have four coupling slots on each side of a coupling cell, and each of them is located azimuthally 90 degree apart from adjacent ones (See Fig. 3.1.2.5.2 for details). The cavity is operated with the π/2 mode so as to have good field stability. The operation frequency is 972 MHz, which is three times as high as that for the lower energy part. This frequency jump is introduced to realize higher acceleration efficiency. The main parameters of the ACS part are summarized in Table 2.1.4.1.1. The ACS part consists of 23 ACS modules, each of which consists of two ACS tanks and one bridge coupler. The layout of an ACS module is shown in Fig. 2.1.4.1.1. One ACS module is driven by one 972 MHz klystron. The RF power is fed through an RF coupler located in the middle of a bridge coupler. One ACS tank consists of 15 accelerating cells and 14 coupling cells. A bridge coupler consists of nine bridge cells, which are also operated with the π/2 mode. An ACS tank and a bridge coupler are connected by an end-coupling cell. The details of the mechanical and RF design of the ACS modules are discussed in Section 3.1.2.5. In this section, we discuss the reason why these fundamental parameters are chosen, and also show some results of beam dynamics simulation.

At first, we determined to adopt a doublet focusing lattice which enables us to have a shorter focusing period and, hence, stronger focusing strength. To ease the space-charge

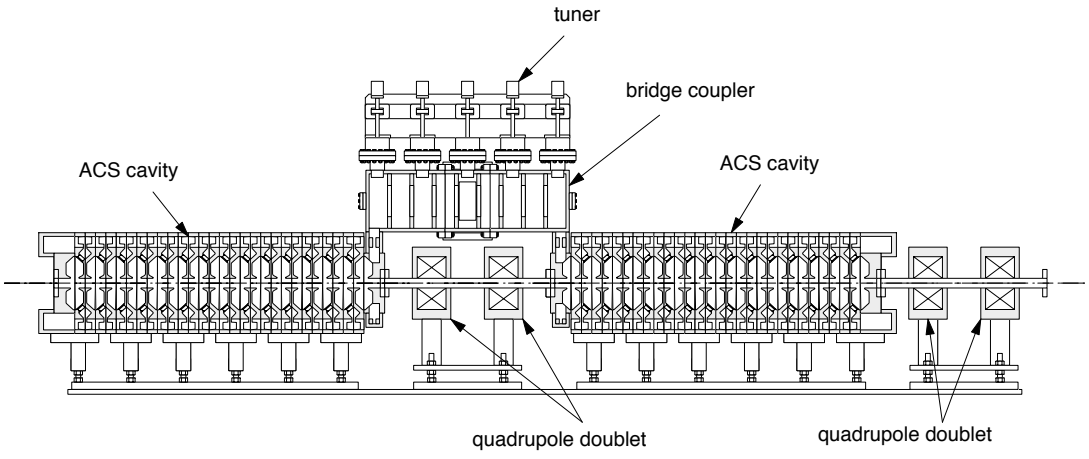

Fig. 2.1.4.1.1. Layout of an ACS module.

Table 2.1.4.1.1. Main parameters of the ACS part

Operation frequency	972 MHz
Input beam energy	190.8 MeV
Output beam energy	400.0 MeV
Number of ACS modules	23
Number of ACS tanks	46
Number of tanks in an ACS module	2
Number of bridge couplers	23
Number of accelerating cells in an ACS tank	15
E_0T	3.52-3.56 MV/m
E_0	4.26 MV/m
E_{smax}/E_k	0.77-0.85
Total peak RF power	43.8 MW
Total peak structure power loss	33.4 MW
Synchronous phase	-30 degree
Drift length between tanks	4.5 $\beta\lambda$
Focusing lattice type	doublet focusing
Number of focusing quadrupoles	90
Focusing period length	12 $\beta\lambda$
Total length	108.3 m

effects, stronger focusing force is preferable. Second requirement is that we can satisfy the equipartitioning condition [3, 4] with a zero-current transverse phase advance of less than 90 degrees. This requirement sets an upper limit for the focusing period length for a given accelerating gradient. The third requirement, which comes from beam dynamics consideration, is the smoothness of focusing and accelerating forces along the ACS part. The smoothness is of essential importance to avoid any deterioration of the beam quality due to space-charge effects. From this point of view, the focusing period scaled by β is kept constant for the entire ACS part. In addition, we determined to have the same E_0 for each ACS tank with E_0 being the average acceleration field strength. The ACS accelerates negative hydrogen beams from 190.8 MeV to 400 MeV. Because the transit time factor T varies only slightly in this energy range, the effective accelerating field E_0T varies smoothly enough along the ACS. The drift length is determined to be 4.5 $\beta\lambda$ considering the required space for a quadrupole doublet, vacuum manifolds, and beam monitors. Then, simply having the same number of cells for all ACS tanks secures sufficient smoothness.

A main restriction in determining the ACS design parameters is the available RF power. We use 972 MHz klystrons as RF power sources for the ACS part. While the maximum saturation power of the klystron is 3.0 MW, we plan to use a klystron with a saturation power of 2.5 MW for stable operation. Then, considering the loss in waveguides and the margin for klystron tuning, the RF power usable in an ACS module is about 2.0 MW. Considering the available RF power, we determined the number of tanks in one RF module to be two. Increasing the number of tanks in one RF module under the above-mentioned limit could have little benefit, considering that it increases the drift space and the RF power

dissipation in bridge couplers. The number of ACS modules and the number of cells in one tank are determined considering the geographical limitations and the construction cost along with the available RF power. Because of a geographical reason, the total length of the ACS part should be shorter than 110 m to have a sufficiently long straight section in the succeeding beam transport line. As for the construction cost, reducing the number of RF modules is the most cost-effective. Taking these factors into consideration, we determined to adopt 23 ACS modules with 15-cell ACS tanks. These parameters give the minimum number of RF modules under the above-mentioned conditions. In this design, E_0 is 4.26 MV/m and the maximum surface field E_{smax} is less than 0.85 E_k with E_k being the Kilpatric limit. The total length of the ACS part is 108.3 m, including inter-tank spacing.

For easy manufacturing, we adopted a "symmetric design" in which all cells in an ACS tank have the same geometrical beta. By adopting a symmetric design, a phase slip of about ± 1.5 degrees is introduced in each ACS tank. We are also considering the possibility of adopting an "extended symmetric design" in which all of the cells in an ACS module (which consists of two ACS tanks) has the same geometrical beta. As the phase slip becomes about ± 6 degrees in this case, we should carefully examine the effect of the phase slip before deciding to adopt this design.

As mentioned above, a doublet focusing lattice is adopted in the ACS part. The quadrupole thickness should be determined so as to suppress beam loss due to the electron stripping of negative hydrogen ions. In the ACS part, the thickness is determined to keep the fractional stripping loss rate lower than 10^{-8} /m. The required thickness depends on the beam energy, and ranges from about 120 to 160 mm. We plan to adopt quadrupole magnets with two or three different thicknesses to effectively utilize the drift space between tanks. The distance between two quadrupoles of a doublet pair was determined to be 300 mm (pole center to pole center) to avoid magnetic field interference. The quadrupole strength is determined to satisfy the equipartitoin condition.

A systematic error analysis is currently in progress using PARMILA [5]. In this analysis, we find the alignment error of the quadrupole magnets and the RF phase/amplitude control errors play dominant roles in determining the output beam quality, while the beam evolution is relatively insensitive to the phase slip and the field tilt in one ACS module.

References

[1] V. G. Andreev et. al., in "Proc. of 1972 Proton Linac Conference", 114 (1972).

[2] T. Kageyama, Y. Morozumi, K. Yoshino and Y. Yamazaki, in "Proc. of The 9th Symposium on Accelerator Science and Technology", Tsukuba, 140 (1993); in "Proc. of The 1994 Internatinal Linac Conference", Tsukuba, 248 (1994).

[3] R. A. Jameson, IEEE Trans. Nucl. Sci., NS-28, 2408 (1981).

[4] M. Reiser, "Theory and design of charged particle beams", John Wiley & Sons, New York (1994).

[5] H. Takeda, Los Alamos National Laboratory Report, LA-UR-98-4478 (1998).

Table 2.1.4.2.1. Main parameters of MEBT2.

Operation frequency	972 MHz
Input beam energy	190.8 MeV
Output beam energy	190.8 MeV
Number of buncher modules	2
Number of ACS tanks in a buncher module	2
Number of accelerating cells in an ACS tank	5
E_0T (Max.)	3.77 MV/m
E_0 (Max.)	4.5 MV/m
Peak voltage integral E_0TL (per module, Max.)	3.23 MV/m
E_{smax}/E_k (Max.)	0.90
Synchronous phase	-90 degree
Inter-tank spacing in a buncher module	2.5 βλ
Focusing lattice type	modified doublet focusing
Number of focusing quadrupoles	12
Total length	15.9 m

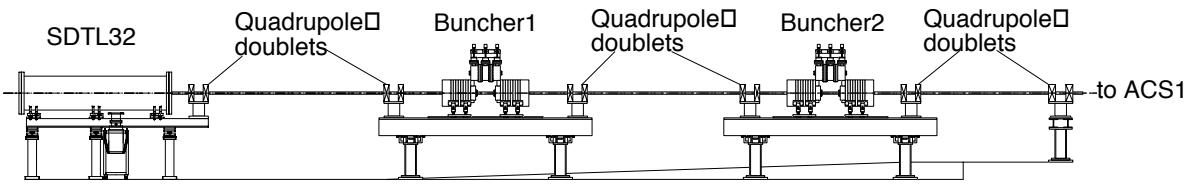

Fig. 2.1.4.2.1. Layout of MEBT2.

2.1.4.2 MEBT2

Initial beam-size mismatch also significantly affects the beam quality. To suppress beam deterioration and excess beam loss, accurate beam matching is indispensable. To make accurate matching, we have a 16 m long beam matching section between the SDTL and the ACS, which we refer to as MEBT2 (Medium Energy Beam Transport 2). The layout of MEBT2 is shown in Fig. 2.1.4.2.1, and the main parameters of MEBT2 are summarized in Table 2.1.4.2.1.

Because both of SDTL and ACS have a doublet focusing lattice for transverse focusing, we adopt a modified doublet focusing lattice for MEBT2, which enables us to perform smooth matching over a wider parameter space. In MEBT2, a quasi-periodic lattice is adopted in which the focusing period length gradually decreases to absorb the difference in the focusing period length between SDTL and ACS. MEBT2 consists of six quadrupole doublets, and the middle four of them are used to perform transverse matching. Two doublets located at both ends are adjusted to find a smoother solution as an auxiliary measure. We prepare independent power supplies for 12 quadrupole magnets to enable the unsymmetrical excitation of a quadruple pair, which secures higher flexibility.

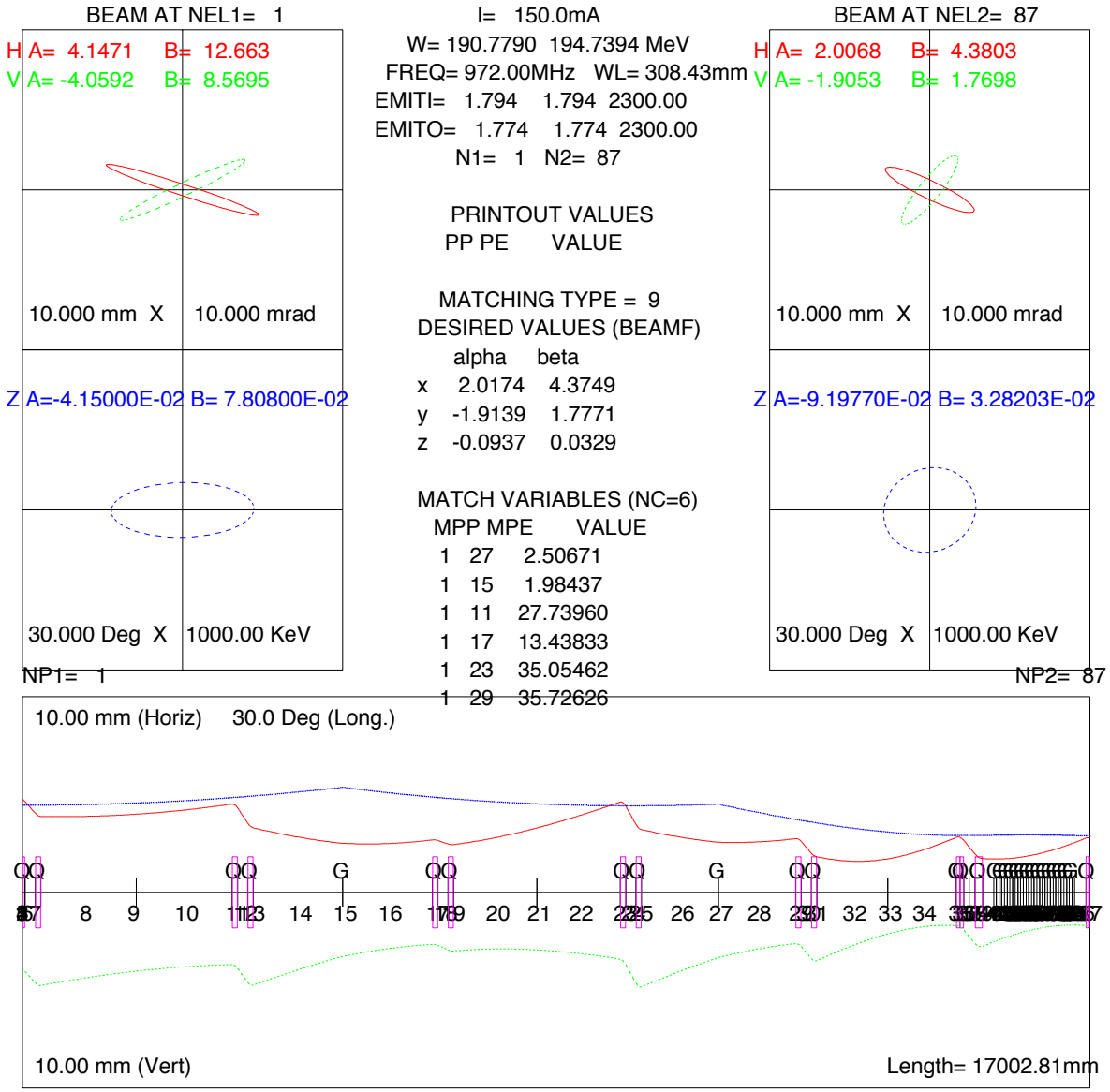

Fig. 2.1.4.2.2. Trace 3D output for MEBT2. In this calculation, the first ACS module is included, and buncher modules are represented by thin RF gaps.

As for longitudinal matching, we have two buncher modules in MEBT2. The main parameters of the buncher modules are summarized in Table 2.1.4.2.2. A buncher module consists of two ACS tanks and one bridge coupler. In an ACS tank, we have five accelerating cells and four coupling cells. A bridge coupler consists of five bridge cells. Except for the number of cells, the buncher module is the same as the nominal ACS module. It should be noted here that the discontinuity of the longitudinal focusing strength between SDTL and ACS, that arises from the frequency jump, should be absorbed in this matching section.

The matching condition is obtained with TRACE 3D [1]. An example of the TRACE 3D output is shown in Fig. 2.1.4.2.2. As demonstrated in this figure, we can find a smooth

matching solution in wide parameter space. Having a beam matching section between SDTL and ACS, we introduce discontinuity of the longitudinal focusing strength, which is not preferable to suppress beam deterioration. Another choice for beam matching is to join SDTL and ACS directly, and smoothly connect the longitudinal focusing strength by introducing an E_0 ramp. While a smooth connection of longitudinal parameters can be realized in this scheme, the transverse focusing period length suddenly changes at the connection point. In addition, we need a long ramp section to absorb the longitudinal focusing strength difference due to the three-times frequency jump, which significantly decreases the acceleration efficiency. As a result, it becomes difficult to fit the ACS into the limited available space. This is the main reason why we introduce a long matching section between SDTL and ACS. Having a matching section is also advantageous for beam diagnosis because it provides space for beam monitors. The detailed configuration of the beam monitor system in MEBT2 is now under consideration.

References

[1] K. R. Crandall and D. P. Rusthoi, Los Alamos National Laboratory Report, LA-UR-97-886 (1997).